

3D Porous Sponge-Inspired Electrode for Stretchable Lithium-Ion Batteries

Wei Liu, Zheng Chen, Guangmin Zhou, Yongming Sun, Hye Ryoung Lee, Chong Liu, Hongbin Yao, Zhenan Bao, and Yi Cui*

Motivated by the rapid development of wearable portable electronics, conformable skin sensors, and implantable medical devices, stretchable high-energy storage has attracted growing attention. Of particular interest are lithium-ion batteries (LIBs) due to high-energy density and broad range of potential applications.^[1–3] In the past decade, many LIBs have been developed with the flexible, bendable, or foldable characteristics,^[4–6] nevertheless, few researches focus on the batteries with advanced feature of stretchability in which the systems are able to accommodate large mechanical strain and still maintain their functions. For LIBs presenting stretchability, a deviation from standard materials is necessary. Including anode, cathode, separator, current collector, as well as packaging material, each component in the stretchable LIBs must withstand deformation. As a core component, identifying a reliable stretchable electrode with good mechanical properties, high electron and lithium-ion conductivity is a significant challenge.

To realize the electrodes for stretchable LIBs, two approaches are usually considered: one is based on materials that have intrinsic stretchable feature and the other one is using structural design that are able to operate under mechanical strain.^[7–16] Currently, the former approach faces significant new materials development, representing a more difficult challenge to be achieved. One alternate for the latter method is loading active materials on stretchable substrates that can maintain conductive paths while being stretched. Conductive materials such as carbon nanotubes (CNTs) and metal nanowires are commonly used to improve the electrical conductivity of the stretchable substrates.^[8–10] With regard to the elastic substrate or scaffold

for flexible and stretchable electronic devices, polydimethylsiloxane (PDMS) is the most widely used elastomeric polymer owing to its unique advantages, including remarkable mechanical flexibility and stretchability, and chemical and thermal stability.^[17,18] Rogers and co-workers^[3] reported stretchable LIBs by using a segmented design in the active materials and deformable electrical interconnects in self-similar geometries. However, the interconnect structures contributed to the deformation of the battery while the component of the electrode remained rigid, which results in a low utility of active materials. Another common design of stretch-tolerant structure is using a “wavy” layout by the processes of buckling, where active materials are coated on a pre-strained elastic substrate.^[11–13] The concept of textile structural configuration together with the design of helically coiled spring is also studied.^[15,16] Although the stretchability is achieved, such 2D structures with low stability under stretching can only be unidirectionally stretched that limits their applications.

So far, reliable stretchable LIBs with high electrochemical performance and good mechanical properties are rarely reported. In the present work, we introduce a novel and simple method to fabricate stretchable electrodes, using highly elastic 3D porous sponge-like PDMS scaffolds. A cost-effective material of sugar is used as a template to generate the stretchable PDMS sponge with open network of pores. Morphologies and electrochemical performances of the stretchable electrodes have been investigated systematically, according to the application in stretchable LIBs.

By using sugar cubes (Figure 1a) as the pore-creating agent, 3D porous sponge-like PDMS scaffolds (Figure 1b, Figure S1, Supporting Information, and Movie 1) with highly stretchability were fabricated.^[19] The PDMS sponge could be sectioned into thin disks (thickness is 500 µm) by a cryostat microtome. As shown in Figure 1c, the stretchable electrodes were then prepared by filling electrode materials including active material, carbon black, and binder in the sponges. Sugar cubes could be either purchased or prepared by pressing sugar powders into a bulk using various molds, which results in the corresponding PDMS sponges with any desired shape and size. The micromorphologies of the PDMS sponges are shown in Figure 1d–f, indicating that the microstructure of the sponge is the inverse matrix of the sugar, in which the pore distribution and orientation formed following the sugar templates. It can also be found from Figure 1f that the average pore size for the sponge could be reduced greatly by using ball-milled sugar powders. It should be noted that the ball milling process using zirconia balls might introduce zirconia contamination in the sugar powders. The zirconia balls and the tank were required to be

Dr. W. Liu, Dr. G. Zhou, Dr. Y. Sun, Dr. C. Liu,
Prof. H. Yao, Prof. Y. Cui
Department of Materials Science and Engineering
Stanford University
Stanford, CA 94305, USA
E-mail: yicui@stanford.edu

Dr. Z. Chen, Prof. Z. Bao
Department of Chemical Engineering
Stanford University
Stanford, CA 94305, USA

Dr. H. R. Lee
Department of Electrical Engineering
Stanford University
Stanford, CA 94305, USA

Prof. Y. Cui
Stanford Institute for Materials and Energy Sciences
SLAC National Accelerator Laboratory
Menlo Park, CA 94205, USA

DOI: 10.1002/adma.201505299



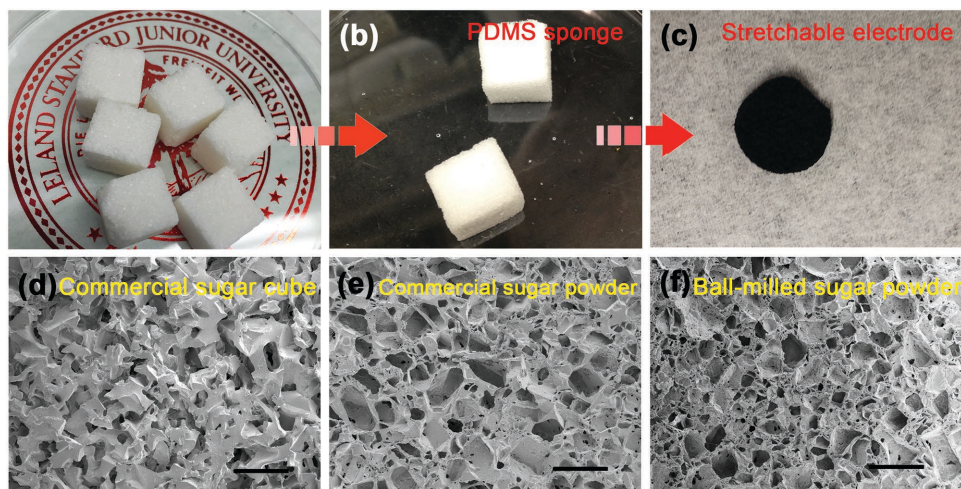


Figure 1. Schematic illustration for the synthesis of the stretchable electrode for LIBs. Digital photographs of a) sugar cubes, b) PDMS sponge, and c) stretchable electrode. SEM images of the PDMS sponges based on d) commercial sugar cubes, e) commercial sugar powders, and f) ball-milled sugar powders. Scale bar: 500 μm .

cleaned carefully to minimize this contamination. Therefore, the cheap and abundant sugar as the template with controlled grain size is very powerful for the fabrication of porous materials, which can realize a wide range of applications. Moreover, the sugar was easy to be removed by dissolving in water and could be recycled after evaporating the water, which is sustainable and cost effective.

In the current work, the $\text{Li}_4\text{Ti}_5\text{O}_{12}$ (LTO) anode and the LiFePO_4 (LFP) cathode have been used as examples to demonstrate the performance and practicability of the stretchable electrode based on the PDMS sponges. The spinel LTO has been investigated as an appealing anode candidate as the insertion of Li ions is at 1.5 V (vs Li/Li⁺), exhibiting small volume changes during cycling with a remarkable stability.^[20,21] Meanwhile, LFP attracts particularly interest owing to its low cost and the environmental compatibility.^[22,23] The LIBs based on LTO/LFP are being commercialized for electric vehicles and energy storage systems. As shown in the top-view scanning electron microscopy (SEM) images (Figure S2, Supporting Information), the morphologies of the stretchable electrodes indicate that the surfaces of the sponges are fully and uniformly covered by the electrode materials (including LTO/LFP, carbon, and binder). The energy dispersive spectroscopy (EDS) mapping of various elements also supports the homogeneous loading of the electrode materials on the PDMS sponges. In addition, the across sectional morphology of the stretchable electrode shown in Figure S3 (Supporting Information) also clearly indicates that the electrode materials were uniformly loaded in the interior region of the PDMS sponge.

A series of electrochemical measurements were carried out on the stretchable electrodes, using half cells with Li-metal as the counter electrode. Together with equivalent circuit, the representative impedance spectra of the stretchable LTO anode and LFP cathode are shown in Figure S4 (Supporting Information), respectively. Each spectrum consists of two semicircles at high and intermediate frequency range and a Warburg tail at low frequency range. It suggests that at high frequency, the resistance R1 from the intercept with the X-axis is attributed to electrolyte,

electrode leads and terminals, and the two semicircles could be ascribed to the interfacial resistances of the electrolyte/LTO interface and the Li/electrolyte interface. The slope at low frequencies corresponds to diffusion-resistance arising from electrode materials.^[24] Similar resistances for the battery using stretchable electrodes compared with the conventional electrodes are observed, which suggests the fast transport channel for charge carriers formed by loading electrode materials on the surfaces of the PDMS sponge with 3D interconnected porous structure is conductive effectively, although the sponge is insulated. Moreover, with novel functionalities of flexibility, stretchability, and lightweight, the superiority of the PDMS sponge is visible, which could be used as flexible, foldable, and stretchable conductors by simple loading conductive materials such as CNTs, graphene, and metal nanowires.

The electrochemical performance of the stretchable electrode in an unstretched state is demonstrated in Figure 2. The typical discharge/charge voltage profiles of the stretchable LTO anode with various active material loadings, together with the date for the conventional LTO electrodes using planar metal foil, are shown in Figure 2a. At a low mass loading ($\approx 1.5 \text{ mg cm}^{-2}$), the conventional electrode on metal foil has advantage over the stretchable electrode, which is due to the low coverage of LTO and carbon in the sponge resulting in a poor electrical contact. However, with increasing the mass loading (3.0 mg cm^{-2}), reduced specific capacity is expected and observed for the cell using the conventional electrode. Nevertheless, it is opposite for the cell using the stretchable electrode (6.0 mg cm^{-2}). This could be easily understood that particle aggregation and non-uniform distribution could be introduced for the electrode using 2D metal foil, while the use of 3D porous sponge could avoid the above issue. Note that further increased loading weight (14 mg cm^{-2}) also leads to reduction of electrochemical performance for the stretchable electrode, as a result of a detachment of electrode materials from the sponge. Despite this the stretchable LTO anode with high mass loading of 14 mg cm^{-2} still remained a high specific capacity of 135 mAh g^{-1} at 0.1 C. Besides the LTO anode, the LFP cathode also exhibits high

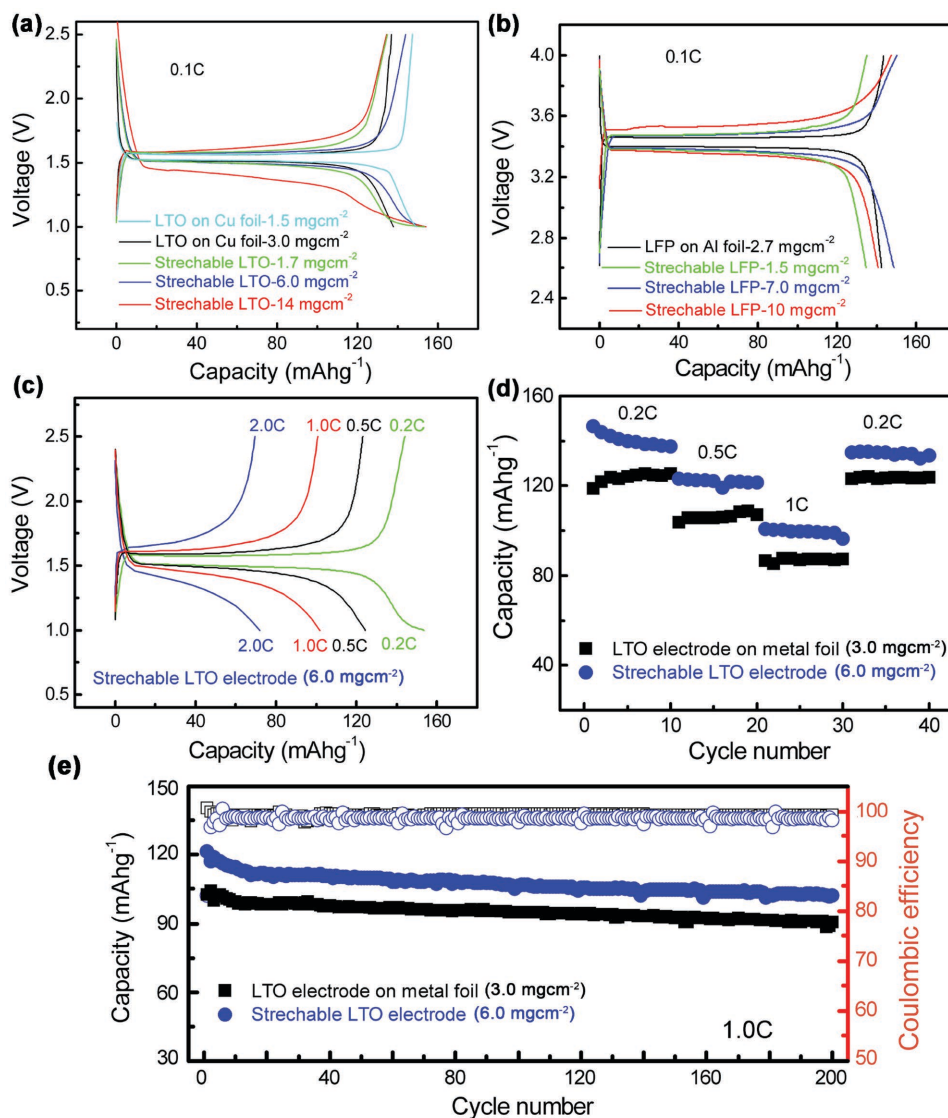


Figure 2. Electrochemical performance of the stretchable electrodes. a) Discharge/charge voltage profiles of the stretchable LTO anode with various loading masses compared with conventional LTO electrode. b) Discharge/charge voltage profiles of the stretchable LFP cathode with various loading masses compared with conventional LFP electrode. c) Discharge/charge voltage profiles of the stretchable LTO anode taken at various C rates. d) Rate capability of the cells using stretchable LTO anode discharged at various current rates from 0.2 to 1.0 C. e) Cycling performance and Coulombic efficiency of the stretchable LTO anode at 1.0 C, together with the data for conventional LTO electrode.

specific capacity and stable cycling performance at various current densities (Figure 2b, Figures S5 and S6, Supporting Information), indicating the robustness and stability of the as-designed electrodes that can be extended to other electrode materials.

Furthermore, Figure 2c gives discharge/charge voltage profiles of the stretchable LTO anode taken at various C rates ranging from 0.2 to 1.0 C (mass loading is around 6.0 mg cm⁻²). In addition, due to the high conductivity retained under charge/discharge cycling, the stretchable LTO electrode also has good rate capability. As shown in Figure 2d, the electrode with stretchable feature is capable to preserve a capacity of 100 mAh g⁻¹ at a rate of 1.0 C, which is higher compared to the conventional LTO foil electrode. Figure 2e shows the Coulombic efficiency (open marker) and cycling performance (solid marker) of the batteries using the

stretchable LTO electrode and the conventional electrode. The former could maintain about a capacity of 100 mAh g⁻¹ at a rate of 1.0 C over 200 cycles. It should be noted that the electrochemical performances of the electrodes, either the conventional electrodes or the stretchable electrodes, shown in current work is not comparable to the typical performance of commercial LTO/LFP materials, which is as a result of the low quality of the purchased powders (Figure S7, Supporting Information).

Thus far, the above results have demonstrated that the stretchable electrodes in the unstretchable state have good electrochemical performances, due to that the 3D interconnected porous structure can guarantee a fast conduction. More importantly, advanced feature of stretchability is shown in the following study. The mass loading for the subsequent experiments is around 6.0 mg cm⁻². Figure 3a indicates the

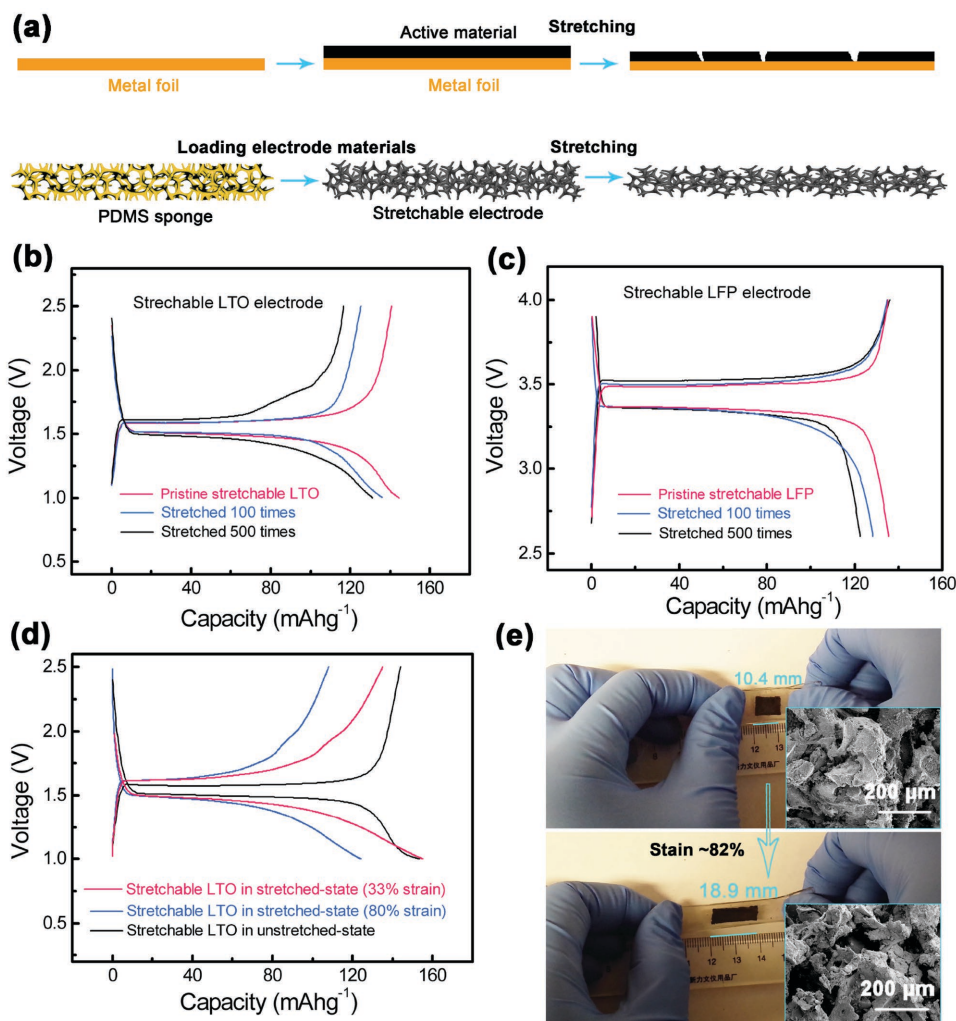


Figure 3. Electrochemical performance and stretchability of the stretchable electrodes. a) Schematic illustration for the comparison of the conventional electrode using metal foil and the stretchable electrode based on the PDMS sponge. Discharge/charge voltage profiles of the stretchable b) LTO anode and c) LFP cathode with various stretch–release cycles. d) Comparison of discharge/charge voltage profiles between the stretchable LTO anode in unstretched state and stretched state with various strains. e) Digital photographs show the electrode with stretchability of $\approx 82\%$. The inset images show SEM images of the electrode in unstretched state and stretched state, respectively.

schematic illustration for the comparison of the conventional electrode using planar metal foil and the stretchable electrode using the sponge-like PDMS. When stretching the conventional electrode, the electrode material may be cracked and dropped off. In other words, the conventional electrode is unable to be deformed. On the contrary, the designed electrode based on PDMS sponge could be stretched without break due to its robust 3D interconnected porous structure. Figure S8 (Supporting Information) clearly shows that the stretchable LTO/LFP electrodes can withstand $\approx 80\%$ strain, which is confirmed in Movies 2 and 3. Furthermore, 500 stretch–release cycles for the stretchable electrode is given in Movie 4, indicating an excellent mechanical property. Also, it is worth noting that the electrode in current work can accommodate strain in all directions, which has more advantages over most studied stretchable conductors (based on buckling structures or helically coiled spring) that can only stretch unidirectionally. In addition, the resistance as a function of the applied strain using different

electrode geometries was shown in Figure S9 (Supporting Information). It can be seen that the resistance first linearly increases six times when the tensile strain increases to 50%, and fully recovers upon release of the strain, using the on-plane electrode. For the second and third cycle of stretch–release, the samples follow almost the same route: the resistance rises up to about eight times and decreases to initial value. Therefore, good stretchability and high reversibility are accomplished for the stretchable electrodes.

Figure 3b,c demonstrates the discharge/charge voltage profiles for the half cells using the stretchable LTO anode and LFP cathode after various stretch–release cycles, respectively, showing 82% and 91% capacity retention after 500 cycles. Compared with the pristine samples, the electrodes by stretch–release cycling show increased voltage hysteresis between the charge and the discharge curves and reduced specific capacity, due to either the nanoparticles aggregation or detachment from the PDMS sponge, resulting in reduced conductivity.

The capacity dependence on cycle number for the stretchable electrode after 500 cycles is shown in Figure S10 (Supporting Information), which indicates excellent cycling performance and high Coulombic efficiency.

To better understand the remarkable electrochemical properties of the stretchable electrode based on the sponge with porous structure, discharge/charge voltage profiles for the half cells using the LTO anode in the stretched status at various strains (33% and 80%) were carried out, as shown in Figure 3d. The capacity retention for the battery using stretched electrode (33% strain) in comparison to unstretched electrode reaches as high as 94%, owing to good ionic and electronic conduction and mechanical property. Digital photographs (Figure 3e) confirm the excellent stretchability of more than 80% for the electrodes. It also indicates from the inset figures of Figure 3e that no obvious change in the micromorphology of the electrode in the stretched state could be observed. Therefore, all the above measurements demonstrate that the stretchable electrodes have good electrochemical as well as mechanical performance, illustrating a broad scope in flexible, bendable, and stretchable LIBs.

The electrochemical performance of the LTO/LFP full cell (using stretchable electrodes) was also evaluated in coin cells prepared as shown in Figure 4. The voltage profile of the LTO/LFP full cell at 0.2 C is the same as that of the cell using conventional electrodes (Figure 4a).^[25] Figure 4b indicates that the full cell cycling performance is especially promising with a capacity retention of about 70% after 300 charge/discharge cycles. Further study on the separator or solid electrolyte and packaging material that could accommodate to deformation would move ahead with plans for LIBs with the functionality of stretchability.

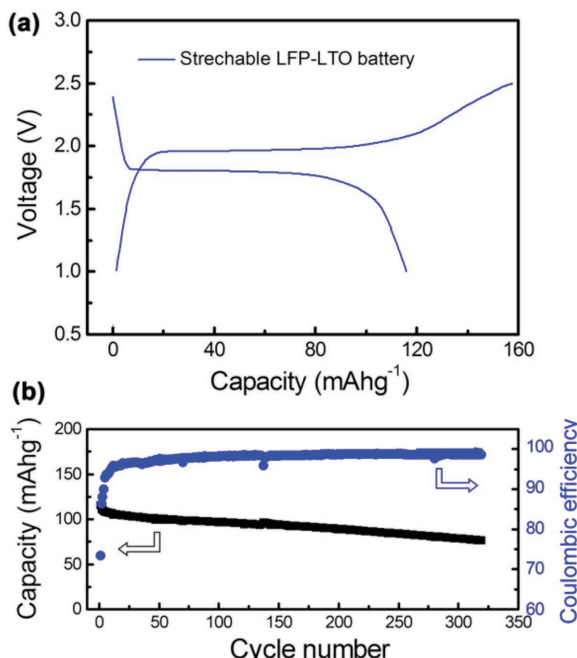


Figure 4. Electrochemical performance of the full battery using the stretchable LTO anode and LFP cathode. a) Discharge/charge voltage profiles, together with b) cycling performance and Coulombic efficiency.

In summary, we have successfully developed stretchable LTO/LFP electrodes by 3D interconnected porous PDMS scaffolds. The sponge-like PDMS was synthesized using a template of cost-effective material of sugar. High active material loading of about 14 mg cm⁻² was achieved for the stretchable electrodes with high specific capacity. The electrodes could effectively offer elastic response to large strain deformations of 80% while maintain good electrochemical performance. 82% and 91% capacity retention for the half cells using the stretchable LTO anode and LFP cathode could be obtained after 500 stretch-release cycles. Additionally, a slight capacity decay of 6% in the battery using the electrode in stretched state is observed. Furthermore, the full cell consists of the stretchable LTO anode and LFP cathode exhibits a stable long-life performance. More importantly, the stretchable electrodes can be easily scaled up for commercial fabrication without complicated procedures at low cost and high efficiency. The current study of the stretchable electrodes for LIBs represents an important potential that will boost the development and application of wearable, bendable, and stretchable electronics.

Experimental Section

Synthesis of Stretchable Electrodes: 3D interconnected porous PDMS sponge was prepared using sugar cube as template. Sugar cubes could be either purchased (Domino Granulated Pure Cane Sugar (15×15×15 mm), Domino Foods, Inc., West Palm Beach, FL, USA) or homemade. For the homemade sugar cube, sugar powders were first filled in a plastic beaker and then dry-pressed into a bulk uniaxially. The grain sizes of the sugar powders could be reduced by planetary ball milling (QM-QX04, Instrument factory of Nanjing University, China) using zirconia balls as the milling medium at a speed of 400 rpm for 30 min. The mixture of silicone elastomer and curing agent at a weight ratio of 10:1 (Sylgard 184, Dow Corning Corporation, Midland, MI, USA) were drop-casted on the sugar cube and infiltrated into the porous structure by capillary force. The Young's modulus of PDMS can be modulated by the ratio of base and curing agent. After curing at atmospheric conditions for 24 h at 50 °C, PDMS on the surface was wiped off till sugar surface exposed. Next, the sugars were dissolved in water and washed away under sonication bath for 5 h. The PDMS sponge was then obtained after drying at 60 °C in vacuum for 10 h. As shown in Movie 1, the sponge is compressible and stretchable. Subsequently, the sponge was sectioned into disks with area of 1 cm² and with thickness of 500 µm by a cryostat microtome (Microm 550M). The thin disks of the PDMS sponge are then treated with argon plasma in an RF plasma chamber (Model MPS-300; March Instruments, Inc., Concord, CA, USA) for 3 min. Electrode slurry consisting of active materials of the Li₄Ti₅O₁₂ (LTO) or LiFePO₄ (LFP) powders (MTI Corporation), carbon black (MTI Corporation), and polyvinylidene fluoride binder (PVdF) (MTI Corporation) with weight ratio of 8:1:1 in N-methyl-2-pyrrolidone (NMP) (Sigma-Aldrich) solvent was drop-casted on the PDMS sponge. For conventional electrodes, the anode or cathode slurry was coated on a Cu or Al foil using a doctor blade. Finally, the samples were dried in a vacuum oven at 70 °C overnight to completely remove the solvent.

Characterization and Electrochemical Measurements: An FEI XL30 Sirion SEM with a field emission gun (FEG) source operated at an accelerating voltage of 5 kV and EDS detector was used to investigate the morphologies of samples. The dependence of resistance on stretchability was conducted on a home-made stretching test station. Stress loading-unloading curves were obtained by using dynamic mechanical analysis (DMA, TA Instrument Q800). The electrical conductivity investigated using AC impedance spectroscopies were recorded by a Biologic VSP potentiostat over the frequency range of 0.10 Hz to 1 MHz. The coin cells (CR2032, MTI Corporation) were assembled using stretchable electrode or conventional electrode, Li metal foil as the counter

electrode, Celgard separator, and 1 M solution of LiPF₆ in EC:DEC (1:1, w/w) liquid electrolyte. All the assemblies were carried out in a dry glove box filled with argon. Galvanostatic measurements are performed using a 96-channel battery tester (Arbin Instruments). For the half cells, the C rate here is calculated based on the theoretical capacity of the electrodes (175 mAh g⁻¹ for LTO and 170 mAh g⁻¹ for LFP). For the full cells, the C rate is used based on the theoretical capacity of LFP. The capacities of the LTO and LFP electrodes in the full cells were matched based on their theoretical capacities. Multiple cells were tested to ensure reproducibility.

Supporting Information

Supporting Information is available from the Wiley Online Library or from the author.

Acknowledgements

This work was supported by Samsung Electronics.

Received: October 27, 2015

Revised: December 16, 2015

Published online:

- [1] R. Bouchet, S. Maria, R. Meziane, A. Aboulaich, L. Lienafa, J. P. Bonnet, N. T. P. Trang, D. Bertin, D. Gigmes, D. Devaux, *Nat. Mater.* **2013**, *12*, 452.
- [2] Z. Chen, W. Ren, L. Gao, B. Liu, S. Pei, H. Cheng, *Nat. Mater.* **2011**, *10*, 424.
- [3] S. Xu, Y. Zhang, J. Cho, J. Lee, X. Huang, L. Jia, J. Fan, Y. Su, J. Su, H. Zhang, H. Cheng, B. W. Lu, C. J. Yu, C. Chuang, T. Kim, T. Song, K. Shigeta, S. Kang, C. Dagdeviren, I. Petrov, P. V. Braun, Y. Huang, U. Paik, J. A. Rogers, *Nat. Commun.* **2013**, *4*, 1543.
- [4] L. Hu, Y. Cui, *Energy Environ. Sci.* **2012**, *5*, 6423.
- [5] Z. Chen, J. W. To, C. Wang, Z. Lu, N. Liu, A. Chortos, L. Pan, F. Wie, Y. Cui, Z. Bao, *Adv. Energy Mater.* **2014**, *4*, 1400207.
- [6] G. Zhou, F. Li, H. M. Cheng, *Energy Environ. Sci.* **2014**, *7*, 1307.
- [7] J. Park, S. Wang, M. Li, C. Ahn, J. K. Hyun, D. S. Kim, J. A. Rogers, Y. Huang, S. Jeon, *Nat. Commun.* **2012**, *3*, 916.
- [8] C. Yu, C. Masarapu, J. Rong, B. Wei, H. Jiang, *Adv. Mater.* **2009**, *11*, 4793.
- [9] Y. Shang, X. He, Y. Li, L. Zhang, Z. Li, C. Ji, E. Shi, P. Li, K. Zhu, Q. Peng, C. Wang, X. Zhang, R. Wang, J. Wie, K. Wang, H. Zhu, D. Wu, A. Cao, *Adv. Mater.* **2012**, *24*, 2896.
- [10] T. Yamada, Y. Hayamizu, Y. Yamamoto, Y. Yomogida, A. Izadi-Najafabadi, D. N. Futaba, K. Hata, *Nat. Nanotechnol.* **2011**, *6*, 296.
- [11] J. A. Rogers, T. Someya, Y. Huang, *Science* **2010**, *327*, 1603.
- [12] Y. Sun, W. M. Choi, H. Jiang, Y. Y. Huang, J. A. Rogers, *Nat. Nanotechnol.* **2006**, *1*, 201.
- [13] W. Weng, Q. Sun, Y. Zhang, S. He, Q. Wu, J. Deng, X. Fang, G. Guan, J. Ren, H. Peng, *Adv. Mater.* **2015**, *27*, 1363.
- [14] S. Wagner, S. Bauer, *MRS Bull.* **2012**, *37*, 207.
- [15] J. Ren, Y. Zhang, W. Bai, X. Chen, Z. Zhang, X. Fang, W. Weng, Y. Wang, H. Peng, *Angew. Chem.* **2014**, *126*, 7998.
- [16] Z. Yang, J. Deng, X. Chen, J. Ren, H. Peng, *Angew. Chem. Int. Ed.* **2013**, *52*, 13453.
- [17] R. Morent, N. D. Geyter, F. Axisa, N. D. Smet, L. Gengembre, E. D. Leersnyder, C. Leys, J. Vanfleteren, M. Rymarczyk-Machal, E. Schacht, E. Payen, *J. Phys. D: Appl. Phys.* **2007**, *40*, 7392.
- [18] T. Sekitani, Y. Noguchi, K. Hata, T. Fukushima, T. Aida, T. Someya, *Science* **2008**, *321*, 1468.
- [19] J. Han, B. Kim, J. Li, M. Meyyappan, *Appl. Phys. Lett.* **2013**, *102*, 051903.
- [20] A. S. Parkas, P. Manikandan, K. Ramesha, M. Sathiya, J. M. Tarascon, A. K. Shukla, *Chem. Mater.* **2010**, *22*, 2857.
- [21] P. Gibot, M. Casas-Cabanas, L. Laffont, S. Levasseur, P. Carlach, S. Hamelet, J. M. Tarascon, C. Masquelier, *Nat. Mater.* **2008**, *7*, 741.
- [22] A. K. Padhi, K. S. Nanjundaswamy, J. B. D. Goodenough, *J. Electrochem. Soc.* **1997**, *144*, 1188.
- [23] A. Yamada, S. C. Chung, K. Hinokuma, *J. Electrochem. Soc.* **2001**, *148*, A224.
- [24] N. Schweikert, H. Hahn, S. Indris, *Phys. Chem. Chem. Phys.* **2011**, *13*, 6234.
- [25] A. Jaiswal, C. R. Horne, O. Chang, W. Zhang, W. Kong, E. Wang, T. Chern, M. M. Doeff, *J. Electrochem. Soc.* **2009**, *156*, A1041.